

# Cable-in-Conduit Dipoles for the Ion Ring of JLEIC

Peter McIntyre , Jeff Breitschopf , Daniel Chavez, Tim Elliott, Raymond Garrison, James Gerity , Joshua Kellams, and Akhdiyov Sattarov

**Abstract**—The electron-ion collider JLEIC requires 3-T arc dipoles with large aperture and homogeneous field suitable for long beam life for all field levels from injection to maximum collision energy. A superferric dipole has been designed using a novel NbTi cable-in-conduit (CIC) conductor and a flux plate to suppress persistent-current multipoles. Fabrication and tests of the 13-kA CIC conductor are presented. A 1.2-m model dipole is under construction, with completion expected in early 2019. Details of the coil technology and magnet fabrication will be presented. A closely similar 6-T dipole has been designed, capable of doubling the ion energy for JLEIC. It utilizes a 2-layer 23 kA CIC cable using the same wire as the single-layer CIC. Fabrication and cable technology for the 2-layer CIC are presented.

**Index Terms**—Collider dipole, cable-in-conduit.

## I. INTRODUCTION

THE Accelerator Research Laboratory (ARL) at Texas A&M University is developing a superferric cable-in-conduit (CIC) dipole for the Ion Ring of Jefferson Lab's proposed Electron-Ion Collider (JLEIC) [1]. JLEIC is a proposed colliding beam facility, responding to the US EIC initiative, in which highly polarized beams of ions and electrons would collide at high energy to study the spin structure of the nucleus. The baseline design for JLEIC was prepared for an ion energy 100 GeV/u, and would require 3 T arc dipoles. ARL has prepared a design for 3 T superferric dipoles using a novel cable-in-conduit (CIC) conductor to provide the large aperture required for the Ion Ring.

A recent NAS study [2] of the physics objectives for EIC found, however, that an ion energy of 200 GeV/u would be required to access the range of physics priorities for the EIC project. Furthermore the collider must be capable of operating with high luminosity over a large range of ion energies in order to cover the dynamics of gluon exchange that connect from present fixed-target studies to the highest collision energy attainable. Motivated by this recent finding, ARL has also prepared a closely similar design for a 6 T CIC-based dipole that would provide the required performance. Both designs are presented.

Manuscript received November 2, 2018; accepted February 15, 2019. Date of publication March 27, 2019; date of current version May 10, 2019. This work was supported by the U.S. Department of Energy, Grant DE-SC0016243. (Corresponding author: Peter McIntyre.)

P. McIntyre, D. Chavez, T. Elliott, R. Garrison, and J. Gerity are with the Accelerator Research Lab, Texas A&M University, College Station, TX 77845 USA (e-mail: mcintyre@physics.tamu.edu; jgerity@tamu.edu).

J. Breitschopf, J. Kellams, and A. Sattarov are with the Accelerator Technology Corporation, College Station, TX 77845 USA (e-mail: akhdiyov@netscape.net).

Color versions of one or more of the figures in this paper are available online at <http://ieeexplore.ieee.org>.

Digital Object Identifier 10.1109/TASC.2019.2907671

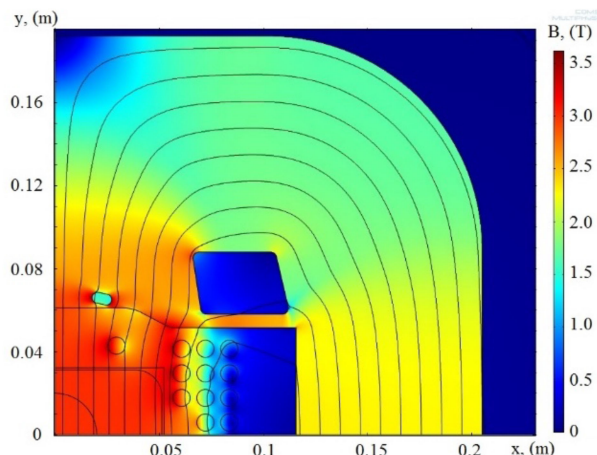


Fig. 1. Quarter cross-section of the 3 T CIC dipole at full field.

The Ion Ring for JLEIC has a Fig. 8 configuration, in which two 260° arcs are connected by two long straight sections. Each arc lattice contains 32 half-cells, and each half-cell contains two 4 m long straight-body dipoles (split to minimize sagitta), a quadrupole, and an instrumentation and correction package.

The required dipole aperture seen by the beam is 10 cm horizontal  $\times$  6 cm vertical. The dipoles must have homogeneity corresponding to all multipoles  $b_n < 10^{-4}$  over the full physical aperture for dipole field  $0.2 \text{ T} < B < 3(6) \text{ T}$ . The wide-aspect-ratio aperture represents a particular challenge for homogeneity and dynamic range.

For this application a superferric block-coil design using a CIC conductor is being developed [3]. The following sections present the magnetic design; the CIC cable design, performance evaluation, and manufacturing issues; and simulation of quench propagation and protection.

## II. 3 T SUPERFERRIC CIC DIPOLE

Fig. 1 shows a cross-section of one quadrant of the 3 T CIC dipole. A total of 24 turns of round CIC cable are wound onto a central structural beam containing a  $10 \times 6 \text{ cm}^2$  stainless steel beam tube. The figure shows contours of the magnetic flux density  $B$  and iso-contours of vector potential for the case of full excitation (3 T). The CIC winding is arranged in 3 equally spaced layers. To correct high field sextupole, one inner turn is relocated from the mid-plane of the dipole to the location  $(x, y) = (3, 4) \text{ cm}$ .

The inner boundaries of the laminated steel flux return are contoured and holes are located as shown to control saturation

TABLE I  
MAIN PARAMETERS OF THE DIPOLES AND CIC CABLES FOR BOTH DESIGNS

Dipole		3 T dipole	6 T dipole	
Bore tube dimensions		10x6	10x6	cm <sup>2</sup>
Coil current	$I_0$	13	23	kA
Operating temp	$T_0$	4.5	4.5	K
Max bore field @S.S.	$B_{max}$	3.6	6.45	T
# turns/pole		12	19	
Stored energy		0.06	0.7	MJ/m
Inductance		0.68	2.5	mH/m
Cable-in-Conduit				
CIC diameter		8.1	11	mm
#strands inner+outer		15	15+21	
Strand diameter	$d_{strand}$	1.2	1.2	mm
Cu:SC stabilizer		1.5:1	1:1	

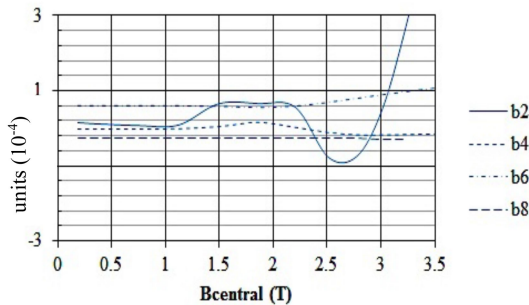


Fig. 2. Calculated systematic multipoles on 2 cm radius reference circle.

over a dynamic range from 0.1 T to 3 T. Table I summarizes the main parameters of the 3 T and 6 T CIC dipoles.

The lattice design requires that systematic multipoles be controlled to a tolerance  $b_n < 10^{-4}$  (expressed in dimensionless units, normalized to  $2/3$  of the magnet aperture radius). This criterion must be maintained over the field range from 0.2 T, where the steel is completely unsaturated, to 3 T, where the inner regions of steel are strongly saturated. Fig. 2 shows the field dependence of the leading multipoles over the full operating range for the 3 T design, extracted from a 2D COMSOL model and verified using Opera2D. The bipolar excursion over the field range 1.5 to 2.8 T arises from the progressive saturation of the inner region of the flux return steel as field is increased. The multipoles are expressed in dimensionless units of  $10^{-4}$ , normalized on a 2 cm radius reference circle. All multipoles are kept to  $< 10^{-4}$  over the entire dynamic range.

#### A. Flux Plate Control of Magnetization Multipoles

A further requirement on field quality is to control persistent-current multipoles and snap-back [4]. Fig. 3 shows the effects of magnetization of the superconducting filaments within the strands of each turn in the CIC winding as the dipole field is increased and decreased. The blue insets show the details of magnetization near two example CIC turns. Shown in red is a horizontal steel flux plate, located above and below the beam tube. At injection field (where persistent-current multipoles are most troublesome) the steel is unsaturated and imposes a strong dipole boundary condition that suppresses all higher multipoles.

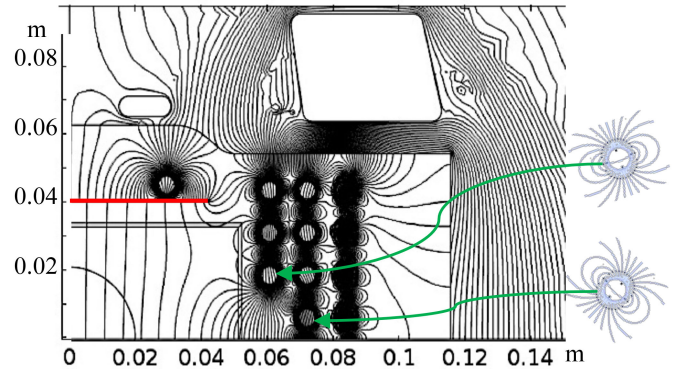


Fig. 3. Addition of steel flux plate (shown in red) to suppress persistent-current multipoles. The vector potential distribution due to residual magnetization of superconducting strands is shown for 0.2 T excitation.

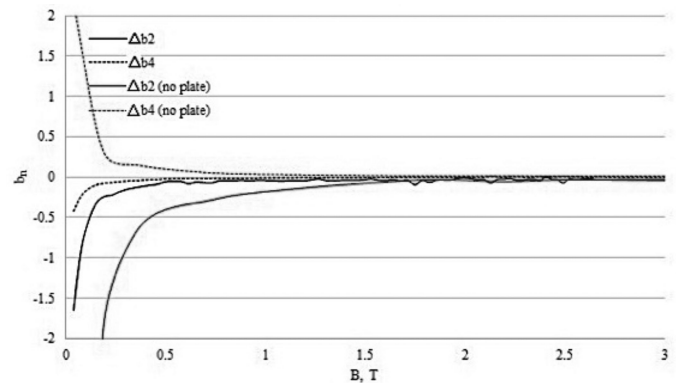


Fig. 4. Snap-back amplitudes for sextupole and decapole over the field range .05– T, with (black) and without (red) the flux plate.

The simulation shown in Fig. 3 shows the distribution of vector potentials arising specifically from the induced magnetizations in the CIC conductors at 0.2 T excitation. Lateral jogs in the potential lines as they pass through the flux plate indicate its benefit in erecting the field and suppressing multipoles.

Fig. 4 shows the step change in the calculated sextupole and decapole amplitudes when the winding current switches from charging to discharging, as a function of field for the dipole with and without the flux plate. The flux plate suppresses the persistent-current sextupole by a factor of 5.

### III. CABLE-IN-CONDUIT

Superconducting Cable-in-conduit (CIC) has been in use for many years for various applications [5]–[8]. The Dubna group [9] developed a ‘cable-outside-conduit’ (COC) for use in their Nuclotron, in which NbTi wires are cabled on the outside surface of a conduit tube and then Nichrome wire is spiral-wrapped over the cable to compress the wires against the conduit tube for thermal contact. Their COC technology was used successfully in the recently completed dipoles for the SIS100 synchrotron at GSI [10]. Although COC cable is successful for the  $\sim 1.8$  T dipoles for Nuclotron and GSI, the limited heat transfer from

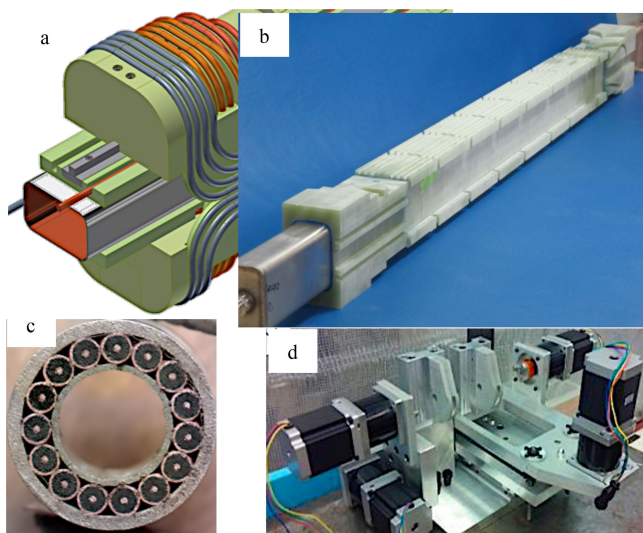


Fig. 5. (a) End region of the 3 T CIC dipole; (b) FRP structural beam; (c) cross-section of 15-strand NbTi CIC; (d) motorized bend fixture used to form the flared ends.

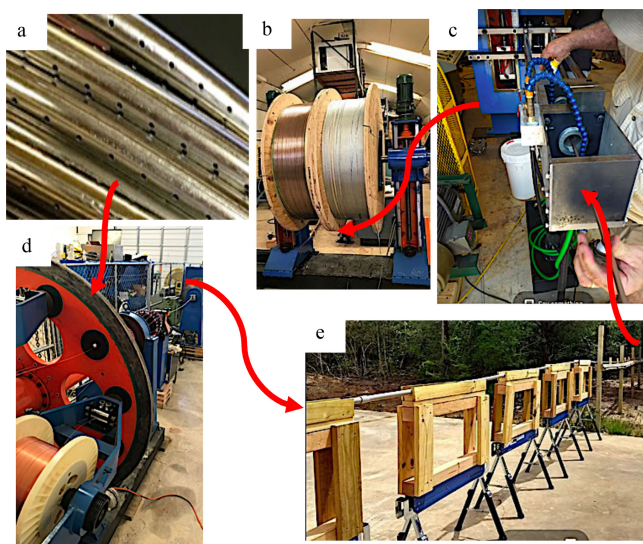


Fig. 6. Fabrication of CIC: (a) perforated 316SS center tube; (b) cable 15 strands of NbTi wire onto center tube, apply 316SS foil over-wrap; (c) pull cable through sheath tube with loose fit; (d) draw sheath tube onto cable.

the wires is problematic for micro-quench stability in magnets requiring higher field and higher stored energy (Section IIIA).

For the JLEIC dipole a true CIC conductor has been developed (Fig. 5c). The fabrication sequence is shown in Fig. 6. A single layer of NbTi/Cu strands is cabled around a perforated thin-wall center tube. An over-wrap of 316 SS tape is applied, the cable is pulled through a loose-fit sheath tube, and the sheath tube is drawn down to compress the strands against the center tube and immobilize them.

The above sequence has been used successfully to fabricate 15-wire CIC segments of 140 m length, suitable to wind the entire winding of a 4 m arc dipole for the Ion Ring of JLEIC.

An alternative method for the sheath formation has been developed by collaborators at HyperTech Research [11], in which the over-size sheath is formed directly onto the cable, the seam is laser-welded, and the sheath tube is drawn to final size. This method transforms CIC manufacture into a continuous process. The formed sheath has been developed so that the laser weld is He-tight. 125 m segments of CIC have been fabricated using the continuous process.

In operation of a CIC winding, liquid helium (LHe) flows within the center tube and bathes all strands through the perforations to provide stability against micro-quenches. The sheath provides stress management at the cable level, so accumulation of Lorentz stress cannot cause degradation of superconducting performance. The sheath also provides a stiff structure, so that flared ends can be formed and, once formed they will sustain their shape thereafter.

An important target of our development was to develop the ability to bend the cable on a 5 cm radius of curvature. The confinement of the wires between the center tube and sheath tube permits the wires to shift in the bend as the inner and outer regions of the bend form different catenary lengths. Several elements of that strategy were crucial to success.

First, we controlled the twist pitch of the cable to equal the arc length of a 90° U-bend with the required curvature. With that choice the catenary lengths of all 15 strands around each bend are equal and no tension or compression is propagated into the straight body segments. This resolved a problem that was encountered in earlier by the INTAS project [12].

Second, after cabling was completed, a thin (25  $\mu\text{m}$ ) foil of stainless steel was spiral-wrapped around the cable to provide a slip plane to facilitate local re-arrangement of the strands during bending. The assembly is then sheathed into a high strength CuNi outer jacket and drawn to a final size in which neighboring wires are in contact and all wires are spring-loaded against the center tube.

Third, the diameters of the center tube and the strands are chosen so that, when the cable is drawn down, the neighboring strands are compressed laterally against one another just as the strands, and at the same time they are compressed radially so that each wire elastically compresses the center tube and is thereby spring-loaded. This dual compression provides for current-sharing between neighboring strands within the cable and decouples external Lorentz stress so that it cannot degrade the performance of wires within the CIC.

Fourth, after drawing, each wire slightly dimples center tube, which contributes to immobilizing each strand against Lorentz forces at high field.

Fifth, a set of motorized bending tools was developed that form the flared end for each winding turn. Fig. 5d shows the tool that forms the 90° flare of the U-bend. A die structure supports the sides of the cable sheath during bending to prevent the oval deformation that would otherwise occur, so that even in a 5-cm radius bend the cable remains almost perfectly round. With all those provisions, we were able to perfect the cable-forming and bending processes and validate by sectioning that the interior configuration remains stable and well-registered throughout a flared end.

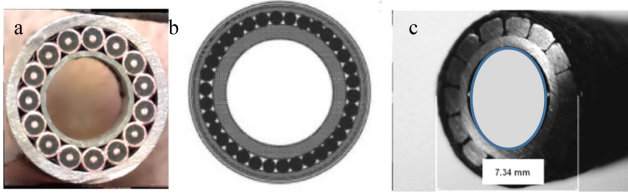


Fig. 7. NbTi cables modeled to estimate MQE and  $T_q$ : (a) CIC for JLEIC, (b) COC with round wires; (c) Dubna/GSI's COC with keystone wires.

A complete winding for the CIC dipole was fabricated onto a precision-machined composite beam made of fiber-reinforced polymer (FRP), shown in Fig. 5b. All bends were formed using the bend tools, and the positions of all cables in the support structure were measured to determine the impact on multipoles from cable position errors. As detailed in Ref. 3, all bends were made successfully and the cable position errors were consistent with  $a_n, b_n < 0.5$  units for all multipoles.

#### A. Enhancement of Micro-Quench Stability in CIC

Quench stability in a superconducting winding determines capital cost (how much superconductor is required) and reliability of operation (all magnets must work without quench on all cycles). Quench typically starts with a micro-quench in one particular place in a winding, and is triggered either by hysteresis jumps or microscopic motions of wires within a cable. Stability depends upon what happens next – does the micro-quench propagate or is the combination of heat transport to cryogen and normal-conducting bypass path for current sufficient to permit it to ‘heal’ back to the superconducting state. The stability against micro-quenches is best characterized by the minimum quench energy (MQE) for a propagating quench [13]. The value of MQE and the recovery time  $T_q$  in which a local micro-quench recovers are the two primary criteria for the stability of a winding.

A simulation has been developed using COMSOL Multi-Physics to compare these criteria for the CIC reported here (Fig. 7a) with two versions of the COC: the original COC using round Nb Ti wires (Fig. 7b) and a version (Fig. 7c) in which the wires are keystone to conform better with the surface of a center tube [14]. The simulation follows heat transfer through the center tube, between neighboring wires, and to LHe; and current redistribution among wires and tubes; as a function of time following a 1 ms micro-quench in a 1 cm segment of one wire.

The contact surface area between adjacent wires and to tube walls was estimated in each case from analysis of the cross section of as-built cable segments. For the CIC each wire-wire contact is 3% of wire surface, and wire-tube contact is 5%. For round-wire COC wire-tube contact is 5% of wire surface for the round-wire version,  $\sim 18\%$  for the keystone version. Heat transfer from walls to LHe was modeled using the Dittus-Boelter equation [15].

In order to estimate MQE for each case, the total heat injected in the micro-quench was adjusted to produce a temperature rise to 10 K. Using that criterion the MQE of the CIC is 10 mJ,

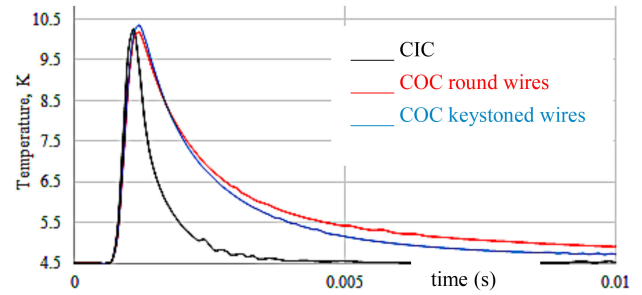


Fig. 8. Time dependence of wire temperature at the end of a wire segment in which a micro-quench pulse is deposited.

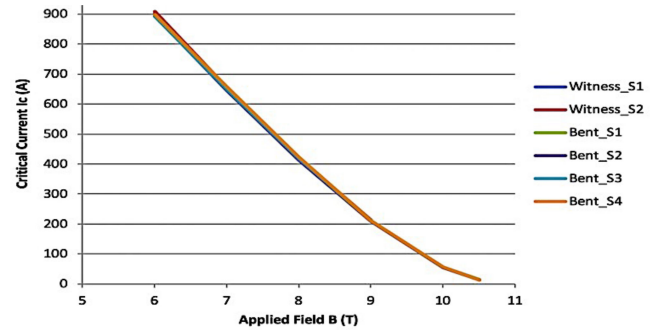


Fig. 9. Measured critical current for extracted strands from U-bends of CIC cable, and for witness strands.

and the MQE for both versions of the COC is 2.4 mJ. Fig. 8 shows the simulated temperature vs. time for all 3 cases. The recovery time  $T_q$  for the CIC to return to 5 K is  $\sim 1.5$  ms for the CIC, 5 ms for the keystone COC, and 7 ms for the round-wire COC. This simulation quantitates that ARL's CIC has greater stability against micro-quenches than either COC, both in MQE threshold heat and in recovery time.

#### B. Testing of Extracted Strands From CIC Cables.

Numerous 2 m-long CIC cable samples were fabricated and formed into final-geometry U-bends. The sheath was then carefully carved open and strands were extracted and tested for potential damage/deformation from cabling, drawing and bending. Some of the extracted strands were tested for current degradation at the Superconducting Magnet Division at Brookhaven National Lab. As shown in Fig. 9, extracted strand performance was equal to that of witness samples. The remainder of samples were etched to check for broken filaments. No filament breakage was observed in any sample.

#### C. Supercritical Helium Flow in CIC Windings

The cryogenics for the CIC dipole has been simulated for the modes of cooldown, collider operation, and quench protection. Supercritical He (SCHe) flows through the perforated center tube and permeates the interstitial spaces among wires within the cable.

SCHe flow is assumed to be manifolded in parallel through the upper and lower halves of each 4 m dipole. The pressure

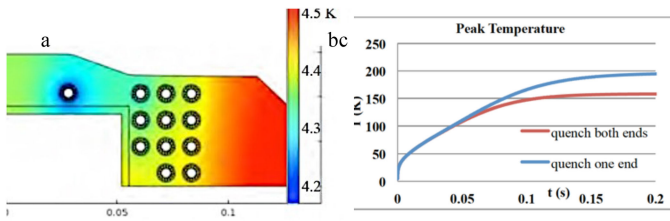


Fig. 10. (a) temperature distribution in CIC winding with 1.8 W heat load and 0.3 m/s SCHe flow; (b)  $T(t)$  following firing quench heaters.

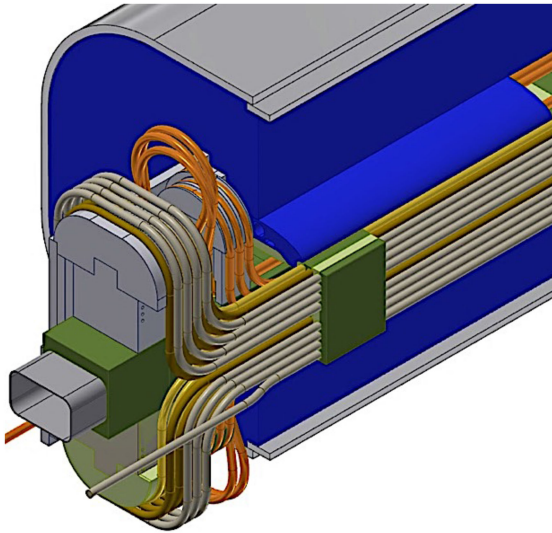


Fig. 11. Cutaway of the end region of the 6 T CIC dipole, showing the end windings and the FRP structure.

drop  $\Delta p$  in the liquid He flow for a  $\sim$ laminar flow in the center tube is

$$\Delta p = f_D \frac{L}{D} \frac{\rho D^2}{2}$$

Where  $D = 4$  mm is the tube diameter,  $L = 104$  m is the half-winding length,  $10^5$  kg/m<sup>3</sup> is the density, and  $f_D = 1.5$  is the friction factor.  $f_D$  was measured experimentally using water flow in a segment of CIC, and agrees with the estimate. The total heat load to one JLEIC dipole is estimated as 1.8 W, using the LHC static heat load of 0.45 W/m/bore. Assuming that heat load a volume flow  $v = 0.3$  m/s would produce a total temperature rise in the dipole of  $\Delta T = 0.3$  K (Fig. 10a). The PV work associated with that SCHe flow is 0.03 W.

Quench protection is integrated onto each end of each turn of the CIC winding, as shown in Fig. 11. Each quench heater is a thin laminar sandwich of Kapton and 50  $\mu$ m thick SS foil. The sandwich is formed to match the crenellations of each cable segment and bonded directly to its sheath tube.

It was assumed that the turns are thermally isolated and a modified version of the QCERN code was used to simulate quench propagation. Estimated quench velocity is 56 m/s. From the MIT's curve it was determined that a 'soak' time of 10 ms is sufficient for thermal diffusion to the superconducting wires after



Fig. 12. Sample of 2-layer CIC, bent on 61 mm bend radius. Inset: cross-section cut on 45° bevel to show inner structure.

firing the quench heaters. Fig. 10b shows the maximum temperature rise for two cases: quench heaters fired from both ends; quench heaters fired from a single end. to a Cu contact block at each end, and bonded to the cable frame. The maximum pressure rise in the CIC cable during a quench is  $\sim 40$  atm.

#### IV. 6 T CIC DIPOLE FOR 200 GeV/u IONS IN JLEIC

The above success with the single-layer CIC and the windings for the 3 T dipole motivated us to develop a design for a CIC-based 6 T dipole that could provide the performance sought in Ref. 2. Fig. 11 shows the design. It utilizes a 2-layer CIC, operating at 23 kA, in which an outer layer of wires is cabled onto the inner layer with reverse twist pitch. The parameters for number of turns and conductor cross-section in the CIC are summarized in Table I.

The biggest challenges for the 2-layer CIC come in fabricating the 2-layer cable with stable registration, and in developing methods and tooling to bend it with the 61 mm bend radius needed for the winding design. Fig. 12 shows a sample of 2-layer CIC with a 61 mm radius bend formed in one end. The inset shows a cutaway on a 45° bevel to show the details of its inner structure.

#### V. SIGNIFICANCE FOR COST AND PERFORMANCE

Willen [16] presented systematic cost estimation methodology for the construction contract of collider dipoles, based upon the experience from building the 4 T dipoles for RHIC. His analysis shows that dipole cost is strongly determined by the number of turns and ends on each dipole and by the quantity of superconductor in the windings. Table II summarizes the two major cost-driver parameters, number of turns/bore and wire cross section, for the 3 T and 6 T CIC dipoles and the IHEP/GSI 6 T cos  $\theta$  dipole. The 6 T CIC dipole (Fig. 11b) requires 19 turns/pole and 8 cm<sup>2</sup>/pole of NbTi wire. The 6 T cos  $\theta$  dipole (Fig. 13a) with the same aperture developed by IHEP for GSI [17] requires 71 turns/pole and 14 cm<sup>2</sup>/pole of NbTi. The CIC-based

TABLE II  
COST-DRIVER PARAMETERS FOR 3 T, 6 T CIC DIPOLES AND 6 T  $\cos \theta$  DIPOLE

	3 T CIC	6 T CIC	6 T $\cos \theta$
Aperture	10 x 6 cm <sup>2</sup>	10 x 6 cm <sup>2</sup>	10 cm round
# turns/bore	12	19	71
Wire cross-section	2.0 cm <sup>2</sup>	7.8 cm <sup>2</sup>	1.7 cm <sup>2</sup>

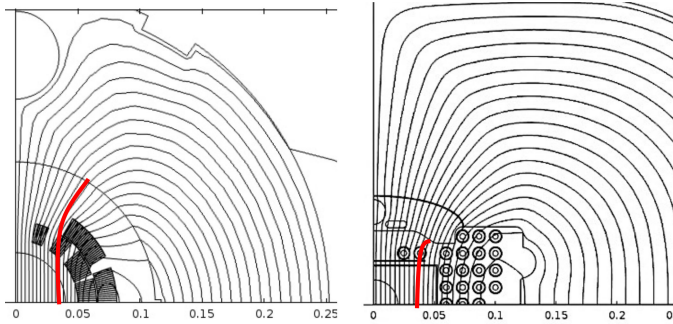


Fig. 13. Two dipoles with same operating field (6 T) and aperture (10 cm): (a)  $\cos \theta$  dipole for SIS-300; (b) CIC dipole for JLEIC.

block winding thus requires half the conductor and one-fourth the turns.

To understand why the CIC-based block winding is so much more amp-efficient than a  $\cos \theta$  winding, one need only consider Ampere's Law around a closed line of force in the two dipoles shown in Fig. 13. Lines of force in the  $\cos \theta$  dipole must travel  $\sim$ twice as far with  $\mu = 1$  (highlighted in red in Fig. 13a) before they enter the flux return steel, compared with those in the CIC dipole (Fig. 13b). The permeability of steel [18] is a big benefit even in saturation ( $\mu = 80$  at 2 T, 3.5 at 3 T, 2 at 4 T, 1.5 at 6 T). The steel is much more closely coupled to the windings in the CIC block-coil geometry, and the aperture can be conformed to the collider requirements (10 x 6 cm<sup>2</sup>).

## VI. CONCLUSION

A novel approach to cable-in-conduit conductor has been developed for use in the arc dipoles of JLEIC. Coil technology has been developed by which the CIC cable can be formed to the flared ends of a dipole winding. Full wire performance and internal cable registration are preserved.

The CIC dipole provides excellent field homogeneity over the large aperture and dynamic range required for JLEIC. Cooling is provided by cryogen flow within the center tube of the CIC, which stabilized the windings to tolerate significant beam losses. A magnetic flux plate is integrated in the structure to suppress multipoles from persistent currents and snap-back by a factor 5.

The CIC dipole was first developed to operate JLEIC with 100 GeV/u ions. A closely similar 6 T CIC dipole, using 2-layer CIC conductor, has been prepared and preliminary development of the required cable is encouraging. The CIC-based block coil

designs provide an efficient, high-performance basis for the requirements of JLEIC using either its baseline design or the enhanced design.

## ACKNOWLEDGMENT

The authors wish to thank Tim Michalski, Probir Ghoshal, Renuka Rajput-Ghoshal, and Ruben Fair of Jefferson Lab for many helpful discussions. Mike Tomsic and Matthew Rindfleisch of HyperTech Research developed the continuous tube forming process that has been successfully implemented for the CIC. Thanks to Arup Ghosh for measurement of critical current in superconducting wire samples at Brookhaven National Lab.

## REFERENCES

- [1] S. Abeyaratne, *MEIC Design Summary*, [Online]. Available: <https://arxiv.org/ftp/arxiv/papers/1504/1504.07961.pdf>
- [2] Committee on U.S.-Based Electron-Ion Collider Science Assessment, *An Assessment of US-Based Electron-Ion Collider Science*, G. Baym, Ed., Washington DC, USA: National Academy Press; 2018, [Online]. Available: <https://www.nap.edu/download/25171>
- [3] JLEIC Arc Dipole Conceptual Design Report, [Online]. Available: <http://arxiv.org/abs/1812.10472>, 2018.
- [4] G. Ambrosio *et al.*, "A scaling law for the snapback in superconducting accelerator magnets," *IEEE Trans. Appl. Supercond.*, vol. 15, no. 2, pp. 1217–1220, Jun. 2005.
- [5] L. Dresner, "Twenty years of cable-in-conduit conductors: 1975–1995," *J. Fusion Energy*, vol. 14, no. 1, pp. 3–12, 1995.
- [6] V. E. Keilin, E. Y. Klimentko, I. E. Kovalev, and B. N. Samoilo, "Force-cooled superconducting systems," *Cryogenics*, vol. 10, no. 3, pp. 224–232, 1970.
- [7] L. Dresner, "Stability of internally cooled superconductors: a review," *Cryogenics*, vol. 20, no. 10, pp. 558–563, 1970.
- [8] V. I. Tronza *et al.*, "Test results of RF ITER TF Conductors in the SULTAN Test facility," *IEEE Trans. Appl. Supercond.*, vol. 24, no. 3, Jun. 2014, Art. no. 4801905.
- [9] N. N. Agapov *et al.*, "Superconducting magnetic system of the fast cycling intermediate energy ion synchrotron," *IEEE Trans. Appl. Supercond.*, vol. 11, no. 1, pp. 1514–1517, Mar. 2001.
- [10] G. Sikler *et al.*, "Fabrication of a prototype of a fast cycling superferic dipole magnet," in *Proc. Part. Accel. Conf.*, Vancouver, 2009, pp. 232–234.
- [11] D. Doll *et al.*, "Method for continuously forming superconducting wire and products therefrom," Patent WO2014109803A2, Jul. 17, 2014.
- [12] V. E. Sytnikov *et al.*, "Development and test of a miniature novel cable-in-conduit conductor for use in fast ramping accelerators with superconducting magnets," *IEEE Trans. Appl. Supercond.*, vol. 16, no. 2, pp. 1176–1179, Jun. 2006.
- [13] M. Breschi *et al.*, "Minimum quench energy and early quench development in NbTi superconducting strands," *IEEE Trans. Appl. Supercond.*, vol. 17, no. 2, pp. 2702–2705, Jun. 2007.
- [14] H. Khodzhbagiyani *et al.*, "Design and test of a hollow superconducting cable based on keystone NbTi composite wires," *IEEE Trans. Appl. Supercond.*, vol. 15, no. 2, pp. 1529–1532, Jun. 2005.
- [15] M. Wilson, *Superconducting Magnets (Monographs on Cryogenics)*, vol. 2, Wotton-under-Edge, U.K.: Clarendon Press, 1983.
- [16] E. Willen, "Superconducting magnets," in *Proc. 34th Eloisatron Workshop*, Erice, Sicily, Nov. 4–13, 1996, BNL-report 64183. [Online]. Available: [https://www.bnl.gov/magnets/magnet\\_files/Publications/BNL-64183.pdf](https://www.bnl.gov/magnets/magnet_files/Publications/BNL-64183.pdf)
- [17] S. Kozub *et al.*, "SIS 300 dipole model," *IEEE Trans. Appl. Supercond.*, vol. 20, no. 3, pp. 200–203, Jun. 2010. [Online]. Available: <https://ieeexplore.ieee.org/document/5430869>
- [18] A. Ito, W. Bosworth, A. T. Visser, J. Grimson, and W. Yang, "B vs. H curves for 1008 and 1020 steels," Fermilab, DuPage County, IL, USA, TM-1197, 1983.